RSC Advances

PAPER

View Article Online
View Journal | View Issue

Cite this: *RSC Adv.*, 2019, **9**, 15791

N-doped graphene/$CoFe_2O_4$ catalysts for the selective catalytic reduction of NO_x by NH_3

Peng Li,[a] Zhifang Li,[bc] Jinxing Cui,[bc] Cui Geng,[a] Yan Kang,[a] Chao Zhang[a] and Changlong Yang *[abc]

In this paper, $CoFe_2O_4$/graphene catalysts and N-doped graphene/$CoFe_2O_4$ ($CoFe_2O_4$/graphene-$_N$) catalysts were prepared using the hydrothermal crystallization method for the selective catalytic reduction of NO_x by NH_3. The results of the test showed that $CoFe_2O_4$/graphene catalysts exhibited the best denitrification activity when the loading was at 4% and the conversion rate of NO_x reached 99% at 250–300 °C. $CoFe_2O_4$/graphene-$_N$ catalysts presented a better denitrification activity at low temperature than $CoFe_2O_4$/graphene catalysts, and the conversion rate of NO_x reached more than 95% at 200–300 °C. The intrinsic mechanism of $CoFe_2O_4$/graphene-$_N$ catalysts in promoting SCR activity was preliminarily explored. The physicochemical properties of the samples were characterized using XRD, TEM, N_2 adsorption, XPS, NH_3-TPD, and H_2-TPR. The results indicated that nitrogen doping can improve the dispersion of $CoFe_2O_4$, and it also increased the acidic sites and the redox performance conducive to improving the denitrification activity of the catalysts. In addition, $CoFe_2O_4$/graphene-$_N$ catalysts demonstrated a better resistance to water and sulfur than $CoFe_2O_4$/graphene catalysts.

Received 1st April 2019
Accepted 14th May 2019

DOI: 10.1039/c9ra02456e

rsc.li/rsc-advances

1. Introduction

Nitrogen oxide (NO_x) is one of the typical atmospheric pollutants.[1] Selective catalytic reduction (SCR) is an effective method to control the emission of nitrogen oxides from coal-fired power plants.[2] At present, V_2O_5–WO_3/TiO_2 catalysts are still widely used in the denitrification process of coal-fired boilers and power plants. However, there are many disadvantages in practical applications, such as high running temperature, poor sulfur and water resistance, and short service life.[3] Therefore, the development of high activity denitrification catalysts at a low temperature is of great significance for environmental protection.

In recent years, iron-based catalysts have been widely used in SCR because of their fine catalytic performance, such as Fe/ZSM-5,[4] Fe/MCM-56,[5] Co–Fe,[6] Fe–Mn,[7] and Co_3O_4–$CoFe_2O_4$@-SiO_2@Au.[8] Among them, Spinel ferrite AFe_2O_4 (A = Zn, Ni, Co, Mn) has the advantages of good chemical stability, high mechanical strength and excellent electromagnetic properties.[9–11] Kennedy *et al.* found that the photocatalytic degradation rate of Rhodamine B by $Co_{0.6}Mg_{0.4}Fe_2O_4$ reached 99.5%.[12] Wang *et al.* found that the photochemical degradation ability of $CoFe_2O_4$/MoS_2 nanocomposites prepared for organic dyes reached 94.9%.[13] The $Co_{1-x}Zn_xFe_2O_4$ nanocomposite studied by Das and co-workers exhibits good photocatalytic properties.[14] Graphene (GE) has been widely used as a carrier to improve the performance of catalysts due to its large specific surface area, high electron mobility and stable chemical properties.[15,16] Yao *et al.* found that $CoFe_2O_4$/graphene has better catalytic activity than $CoFe_2O_4$ in phenol degradation.[17] Bian *et al.* found that $CoFe_2O_4$/graphene nanocomposites exhibit excellent catalytic activity in redox reactions.[18]

N-doped mesoporous carbon materials have been widely used in catalytic reactions. The modification of mesoporous carbon by incorporating nitrogen leads to the better particle dispersity, but also probably disturbs the electronic structure of carbon solids owing to the formation of a semiconductor-like energy gap.[19] To the best of our knowledge, the research of N-doped graphene/$CoFe_2O_4$ ($CoFe_2O_4$/graphene-$_N$) for NH_3-SCR has been rarely reported. In this paper, graphene as catalysts carrier was used to prepare $CoFe_2O_4$/graphene catalysts for NH_3-SCR reaction. The proper proportion of $CoFe_2O_4$/graphene catalysts was determined, and the effect of nitrogen doped on the denitrification performance of $CoFe_2O_4$/graphene catalyst was also investigated. The mechanism of $CoFe_2O_4$/graphene-$_N$ catalyst in promoting SCR activity was preliminarily explored, which provided a theoretical basis for the practical application of AFe_2O_4 catalysts in NH_3-SCR reaction.

[a]*College of Chemistry and Chemical Engineering, Qiqihar University, Qiqihar 161006, Heilongjiang, China. E-mail: changlongy@163.com; Fax: +86 452 2738206; Tel: +86 452 2738206*

[b]*College of Materials Science and Engineering, Qiqihar University, Qiqihar 161006, Heilongjiang, China*

[c]*Heilongjiang Provincial Key Laboratory of Polymeric Composite Material, Qiqihar 161006, Heilongjiang, China*

2. Experimental

2.1 Catalysts preparation

2.1.1 Preparation of GO. Graphene oxide was prepared using the Hummers' method.[20] The preparation process was as follows: 5 g of graphite powder, 2.5 g of sodium nitrate and 115 ml of concentrated sulfuric acid were firstly added to a three-necked flask placed in an ice water bath for stirring, and after being uniformly mixed, 15 g of potassium permanganate was added. The mixture was kept in the ice-water bath for 2 hours, and then transferred from the flask into the thermostat water bath again, and stirred for 30 min at 35 °C. Transfer the mixture in the three-necked flask into an ice water bath and then add 230 ml of deionized water. Finally, react at a constant temperature of 98 °C for 20 min. The reaction mixture was then cooled down naturally to room temperature. Subsequently, the hydrogen peroxide (50 ml) was added and stirred for 10 min. Wash and dry with HCl and deionized water, respectively.

2.1.2 Preparation of $CoFe_2O_4$/graphene and $CoFe_2O_4$/graphene-$_N$ catalysts. The $CoFe_2O_4$/graphene catalysts was prepared by the hydrothermal method.[21] 0.12 g GO was added to 60 ml anhydrous alcohol under ultrasonic for 30 min, as solution A. Another solution was to add a certain amount of cobalt nitrate and ferric nitrate to 20 ml absolute alcohol, namely solution B. Solution B was then added to solution A, and stirred for 30 minutes; after that, 2.16 g sodium acetate was added to continue stirring for 30 minutes, by then crystallized at 200 °C for 12 hours. In the meantime, the loads of $1CoFe_2O_4$/graphene, $4CoFe_2O_4$/graphene, $7CoFe_2O_4$/graphene and $11CoFe_2O_4$/graphene were prepared by changing the amount of cobalt nitrate and ferric nitrate added respectively. Adding solution B into A and adding 1 ml ammonia to prepare $CoFe_2O_4$/graphene-$_N$, the preparation process is the same as above.

2.2 Evaluation of denitrification activity of the catalysts

The denitrification activity of the catalysts was tested with Shanghai Jiangke QJK45 denitrification experimental facility with 0.3 g catalysts. N_2 was used as balanced gas; NH_3 500 ppm; NO 500 ppm; SO_2 100 ppm; O_2 5%; H_2O 3%; the total gas flow was 100 ml min^{-1}; the reaction temperature was 150–400 °C. The conversion rate of NO_x was calculated according to the content of NO_x at the inlet and outlet at 150, 200, 250, 300, 350 and 400 °C respectively. The NO_x content of the inlet gas was marked as $[C_{NO_x}]_{in}$, and the NO_x content of the outlet gas was marked as $[C_{NO_x}]_{out}$. NO_x conversion rate is calculate as:

$$NO_x \text{ conversion}\% = \frac{[C_{NO_x}]_{in} - [C_{NO_x}]_{out}}{[C_{NO_x}]_{in}} \times 100\% \quad (1)$$

2.3 Catalysts characterization

The crystal structure of the catalysts was characterized by Smart lab X-ray diffraction (XRD) of Nippon Science Corporation, with a scanning range of 5–80 degree, an operating current of 200 mA and an operating voltage of 45 kV. Hitachi H-7650 transmission electron microscopy (TEM) was used to characterize the microstructures of the samples (resolution 0.2 nm, acceleration voltage 40–120 kV, magnification 60 000×). The specific surface area, pore size distribution and pore volume of the catalysts was characterized by Autosorb IQ of Conta Instruments Company, USA. Thermo Fisher's ESCALAB250XI X-ray photoelectron spectroscopy (XPS) was used to characterize the surface chemical composition and the chemical state of each element. The surface acidity of the catalysts was characterized by temperature programmed desorption (NH_3-TPD) of AutoChem 2920 NH_3, an American company. AutoChem 2920 H_2 temperature programmed reduction (H_2-TPR) was used to characterize and analyze the redox performance of the catalysts.

3. Results and discussion

3.1 Structure and microstructure analysis of catalysts

Fig. 1 shows the XRD patterns of the graphene oxide (GO), $CoFe_2O_4$, $CoFe_2O_4$/graphene, and $CoFe_2O_4$/graphene-$_N$. The XRD diagram of GO in Fig. 1(a) finds the strong diffraction peak of GO appears at 12 degrees, which indicates that the oxide of graphite has been successfully synthesized.[22] It can be seen from Fig. 1(a) that the obvious diffraction peaks are observed at 30.0, 35.4, 43.4, 57.1 and 62.7 degrees respectively. According to the PDF card, namely PDF#03-0864, $CoFe_2O_4$ has been successfully synthesized. Fig. 1(b) XRD patterns of $CoFe_2O_4$/graphene catalysts with different $CoFe_2O_4$ loadings show that

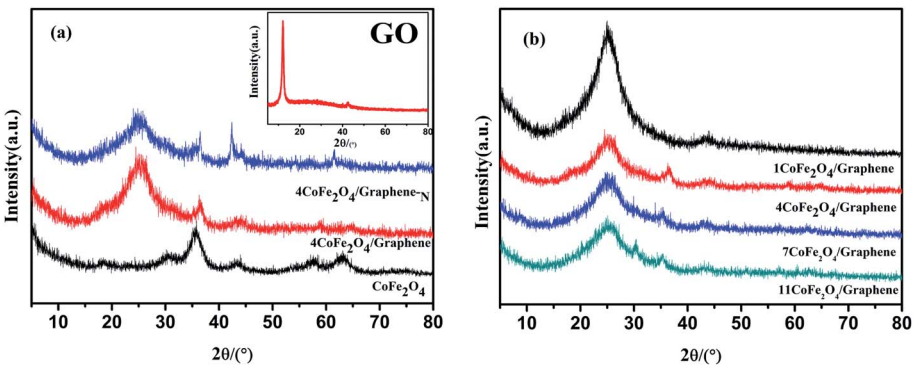

Fig. 1 XRD patterns of (a) GO, $CoFe_2O_4$, $CoFe_2O_4$/graphene, $CoFe_2O_4$/graphene-$_N$, (b) $CoFe_2O_4$/graphene catalysts with different loadings.

there are obvious characteristic peaks of graphene at 25.2 degrees,[23] proving that graphene oxide has been successfully reduced during the preparation of the catalysts. At the same time, the diffraction peaks of $CoFe_2O_4$ can be observed, indicating that $CoFe_2O_4$/graphene catalysts has been successfully synthesized.

Fig. 2 reveals $CoFe_2O_4$ nanoparticles distribute on the surface of graphene. From the TEM diagram of $CoFe_2O_4$/graphene, it can be found that the active components are aggregated, and the distribution of $CoFe_2O_4$ in $CoFe_2O_4$/graphene-$_N$ catalysts is more uniform. The results show that nitrogen doped was beneficial to the uniform distribution of the active components and to make a good contact with the reactants in NH_3-SCR test, thereby enhancing the reactivity of the catalysts.

Fig. 3 shows nitrogen adsorption–desorption isotherms of $CoFe_2O_4$/graphene and $CoFe_2O_4$/graphene-$_N$. It can be seen from the diagram that all types of catalytic isotherms are IV type and the lagging ring type is H1 type. The results show that the catalysts of $CoFe_2O_4$/graphene and $CoFe_2O_4$/graphene-$_N$ contain typical mesoporous structures, and the isotherm hysteresis is related to the existence of voids.

Table 1 is the specific surface area, pore volume and pore size parameters of GO, $CoFe_2O_4$/graphene and $CoFe_2O_4$/graphene-$_N$ catalysts. It was found that the specific surface area of $CoFe_2O_4$/graphene-$_N$ catalysts was reduced, but its denitrification activity was higher than that of $CoFe_2O_4$/graphene catalysts. This indicated that the denitrification activity of the catalysts was not only related to the specific surface area but also to the acidic site and redox performance of the catalysts.

3.2 Nitrogen-doped enhances the denitrification activity of $CoFe_2O_4$/graphene-$_N$ catalysts

Fig. 4 shows the $CoFe_2O_4$/graphene catalysts of different loadings and the denitrification activity of $CoFe_2O_4$/graphene-$_N$. It can be seen from the graph that the denitrification activity of $CoFe_2O_4$/graphene catalysts with different loading amount increases with the increase of the reaction temperature when it is less than 250 °C. When the reaction temperature is at 250 °C, the conversion of NO_x of all catalysts is above 95%, which indicates that the catalysts have good denitrification activity at low temperature. The SCR catalytic activity of $CoFe_2O_4$/graphene catalyst increases and then decreases with the increasing of the loadings. Compared with $CoFe_2O_4$/graphene catalysts of 1%, 7% and 11% loading respectively, $CoFe_2O_4$/graphene catalysts with 4% loading have the highest denitrification conversion in the range of 200–400 °C, indicating that the optimum loading of the prepared $CoFe_2O_4$/graphene catalysts was 4%. Compared with 4$CoFe_2O_4$/graphene catalysts, 4$CoFe_2O_4$/graphene-$_N$ catalyst exhibits higher denitrification activity at low temperature in the range of 150–300 °C. It is due to the more uniform distribution of $CoFe_2O_4$ after nitrogen doped. It is also related to the acidic site, redox performance of the catalysts and the synergetic effect between $CoFe_2O_4$ and N-doped graphene support. The literature reported the synergetic effect can enhance photocatalytic activity and photostability.[25,26] Compared with the reported supported catalysts, $CoFe_2O_4$/graphene-$_N$ catalysts have better denitrification activity (Table 2).[27–29]

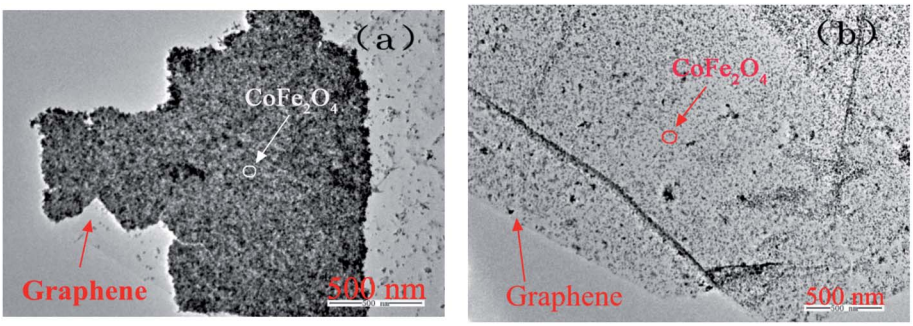

Fig. 2 TEM patterns of $CoFe_2O_4$/graphene (a) and $CoFe_2O_4$/graphene-$_N$ (b).

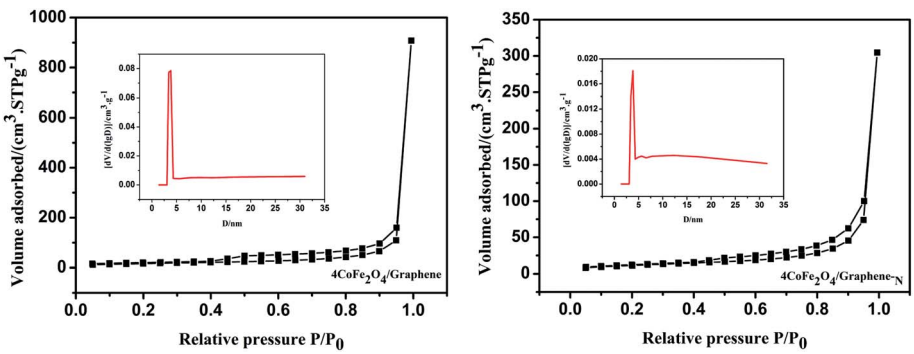

Fig. 3 Nitrogen adsorption–desorption isotherms of $CoFe_2O_4$/graphene and $CoFe_2O_4$/graphene-$_N$.

Table 1 The specific surface area, pore volume and average pore size of GO, $CoFe_2O_4$/graphene and $CoFe_2O_4$/graphene-$_N$

Sample	S_{BET} ($m^2\ g^{-1}$)	V_{Total} ($cm^3\ g^{-1}$)	Average pore size (nm)
GO[24]	337	1.290	3.820
$CoFe_2O_4$/graphene	58	0.268	3.828
$CoFe_2O_4$/graphene-$_N$	40	0.158	3.825

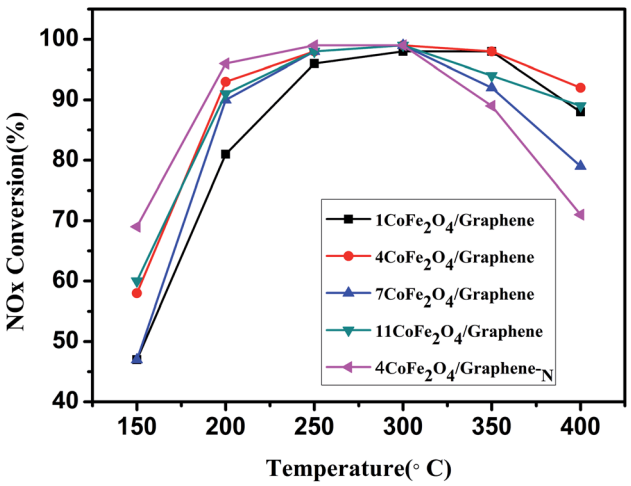

Fig. 4 NH_3-SCR activity of $CoFe_2O_4$/graphene catalysts with different loadings and $CoFe_2O_4$/graphene-$_N$ catalysts. Reaction conditions: NH_3 (500 ppm), NO (500 ppm), O_2 5%, N_2 as balanced gas, total gas flow (100 ml min^{-1}).

3.3 Nitrogen-doped enhances the denitrification mechanism of $CoFe_2O_4$/graphene-$_N$ catalysts

Fig. 5(a) is a wide scan of XPS spectrum of $CoFe_2O_4$/graphene and $CoFe_2O_4$/graphene-$_N$. The binding energy at 284.6 eV, 529.8 eV, 711.6 eV and 780.9 eV attributes to C 1s, O 1s, Fe 2p and Co 2p, respectively.[30] Fig. 5(b) is a C 1s XPS diagram of $CoFe_2O_4$/graphene and $CoFe_2O_4$/graphene-$_N$. The peaks at 284.6 eV and 286.5 eV belong to the C=C and C–O functional groups of graphene, respectively.[31] The C–N bonds were also detected at 285.6 and 287.1 eV, which is attributed to sp^2 and sp^3 bonded C–N, respectively.[32] Fig. 5(c) is a Fe 2p XPS diagram of $CoFe_2O_4$/graphene and $CoFe_2O_4$/graphene-$_N$. The Fe 2p spectrum shows two peaks at 711.1 eV and 725.1 eV, which can be assigned to Fe $2p_{3/2}$ and Fe $2p_{1/2}$, respectively, indicating the presence of Fe^{3+}.[33] Fig. 5(d) is a Co 2p XPS diagram of $CoFe_2O_4$/graphene and $CoFe_2O_4$/graphene-$_N$. The Co 2p spectrum shows two peaks at 781.0 eV and 786.6 eV, which can be attributed to Co $2p_{3/2}$ and its satellite peak. Other peaks are observed at 796.6 eV and 802.8 eV corresponding to the Co $2p_{1/2}$ and its satellite peak, indicating the presence of Co^{2+}.[34] It indicates that $CoFe_2O_4$/graphene and $CoFe_2O_4$/graphene-$_N$ catalysts have been successfully synthesized, which is consistent with the XRD results. Fig. 5(e) is the N 1s XPS diagram of $CoFe_2O_4$/graphene-$_N$. The peak at 398.8 eV belongs to pyridinic nitrogen; the peak at 399.8 eV belongs to pyrrolic nitrogen; and the peak at 401.6 eV belongs to graphitic nitrogen.[35] Table 3 exhibits the percentage of pyridinic nitrogen, pyrrolic nitrogen, graphitic nitrogen for the $CoFe_2O_4$/graphene-$_N$ according to the XPS. The percentage of pyridinic nitrogen, pyrrolic nitrogen, graphitic nitrogen for $CoFe_2O_4$/graphene-$_N$ is 42.42%, 35.89% and 21.69%, respectively. Among the three nitrogen species, pyridinic nitrogen is considered as the main active site for catalyzing oxygen reduction reaction, which can effectively improve the catalytic performance of $CoFe_2O_4$/graphene-$_N$.[36] Fig. 5(f) is the O 1s XPS diagram of $CoFe_2O_4$/graphene and $CoFe_2O_4$/g-$_N$. The characteristic peaks of lattice oxygen (O_β) at 530.4 eV, adsorb oxygen (O_α) at 531.7 eV and surface oxygen (O_γ) at 533.6 eV can be clearly seen from Fig. 5. It can be seen that the adsorbed oxygen (O_α) ratio is calculated by $O_\alpha/(O_\alpha + O_\beta)$ for $CoFe_2O_4$/graphene and $CoFe_2O_4$/graphene-$_N$. The calculated O_α ratio (42.9%) of $CoFe_2O_4$/graphene is slightly higher than that (40.3%) of $CoFe_2O_4$/graphene-$_N$. Surface adsorbed oxygen (O_α) has higher mobility than lattice oxygen (O_β) in SCR reaction,[37] which is helpful to improve the denitrification activity of catalysts, which is consistent with the test results of denitrification activity of catalysts. It means that the high denitrification activity of the $CoFe_2O_4$/graphene-$_N$ catalysts is related to other factors.

Fig. 6 is the NH_3-TPD diagram of $CoFe_2O_4$/graphene and $CoFe_2O_4$/graphene-$_N$. It can be seen that $CoFe_2O_4$/graphene and $CoFe_2O_4$/graphene-$_N$ catalysts have two desorption peaks. Comparing the two curves, $CoFe_2O_4$/graphene-$_N$ catalysts have higher peak temperature and peak area than $CoFe_2O_4$/graphene catalysts. This indicates that the acid strength and quantity of $CoFe_2O_4$/graphene-$_N$ catalysts are superior to that of $CoFe_2O_4$/graphene catalysts, and the increase of acid sites of catalysts promotes the denitrification activity of catalysts.[38]

Fig. 7 is the H_2-TPR diagram of $CoFe_2O_4$/graphene and $CoFe_2O_4$/graphene-$_N$ catalysts. As is shown, the reduction peaks of $CoFe_2O_4$/graphene and $CoFe_2O_4$/graphene-$_N$ catalysts occur at 462 °C and 388 °C respectively. Compared with $CoFe_2O_4$/graphene, the peak of $CoFe_2O_4$/graphene-$_N$ moved to low temperature, indicating that the catalysts have better reduction performance at low temperature. In addition, the reduction peak area of $CoFe_2O_4$/graphene-$_N$ catalysts increases, indicating that the redox performance of the catalysts increases, thus increasing the denitrification activity of the catalysts.[39]

Table 2 The catalytic activities of the reported denitrification catalysts

Catalysts	NO_x conversion (temperature range)	GHSV	References
Cu-ZSM-5	≥80% (250–350 °C)	80 000 h^{-1}	27
CeO_2–ZrO_2/TiO_2	≥80% (250–350 °C)	71 400 h^{-1}	28
CeO_2/Al_2O_3	≥90% (300–400 °C)	7200 h^{-1}	29

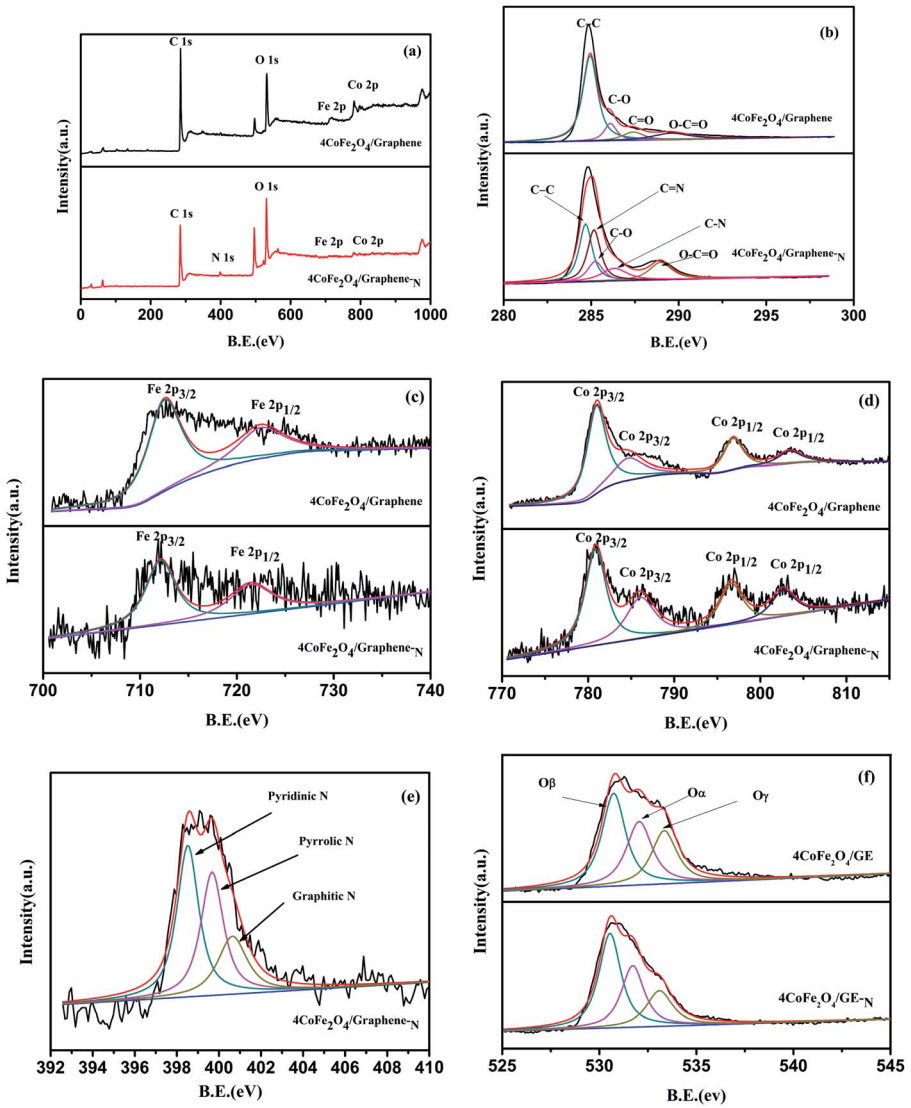

Fig. 5 (a) XPS spectra of $CoFe_2O_4$/graphene and $CoFe_2O_4$/graphene-$_N$ (b) C 1s XPS spectra of $CoFe_2O_4$/graphene and $CoFe_2O_4$/graphene-$_N$ (c) Fe 2p XPS spectra of $CoFe_2O_4$/graphene and $CoFe_2O_4$/graphene-$_N$ (d) Co 2p XPS spectra of $CoFe_2O_4$/graphene and $CoFe_2O_4$/graphene-$_N$ (e) N 1s XPS spectra of $CoFe_2O_4$/graphene-$_N$ (f) O 1s XPS spectra of $CoFe_2O_4$/graphene and $CoFe_2O_4$/graphene-$_N$.

3.4 Test of water and sulfur resistance of $CoFe_2O_4$/graphene and $CoFe_2O_4$/graphene-$_N$ catalysts

Fig. 8 is a test of water and sulfur resistance of $CoFe_2O_4$/graphene and $CoFe_2O_4$/graphene-$_N$ catalysts. It is obvious that the denitrification activity of $CoFe_2O_4$/graphene-$_N$ is higher than that of $CoFe_2O_4$/graphene, indicating that nitrogen doped is beneficial to improving the water and sulfur resistance of the catalysts. The denitrification activity of $CoFe_2O_4$/graphene and $CoFe_2O_4$/graphene-$_N$ catalysts is tested in the presence of SO_2. The denitrification conversion rate of $CoFe_2O_4$/graphene-$_N$ catalysts is relatively poor when the reaction temperature is below 250 °C. The reason was that SO_2 reacts with NH_3 to form sulfate that covers the active sites of the catalysts and blocks the channels of the catalysts, which weakens the catalytic activity. At the high temperature, SO_2 on the surface of the catalysts is converted to SO_4^{2-}, resulting in the increase of surface acidity of the catalysts and the enhancement of the denitrification activity of the catalysts.[40] The poor water resistance of $CoFe_2O_4$/graphene and $CoFe_2O_4$/graphene-$_N$ catalysts is attributed to the competitive adsorption of H_2O and reactive gases (NH_3, O_2, NO)

Table 3 Percentage of pyridinic nitrogen, pyrrolic nitrogen, graphitic nitrogen of $CoFe_2O_4$/graphene-$_N$ from the XPS

Catalysts	Pyridinic nitrogen/%	Pyrrolic nitrogen/%	Graphitic nitrogen/%
$CoFe_2O_4$/graphene-$_N$	42.42%	35.89%	21.69%

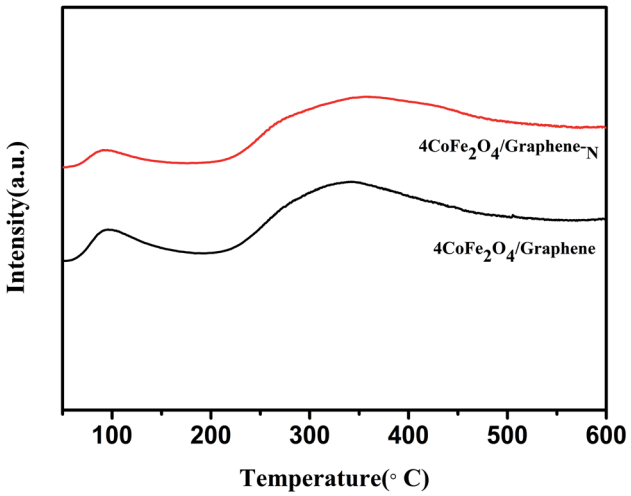

Fig. 6 NH_3-TPD diagram of $CoFe_2O_4$/graphene and $CoFe_2O_4$/graphene-$_N$.

on the surface of the catalysts, and the hydroxyl groups generated by the adsorbed water on the surface of the catalysts neutralize the acidic sites on the surface of the catalysts, resulting in the deterioration of the denitrification activity of the catalysts.[41]

3.5 Repeatability test of $CoFe_2O_4$/graphene-$_N$ catalyst

Fig. 9 shows the repeatability of $CoFe_2O_4$/graphene-$_N$ catalyst for four times. It can be seen from the Fig. 9 that the denitrification activity of the reused $CoFe_2O_4$/graphene-$_N$ (four times) significantly decreased under 250 °C compared with the fresh catalyst. However, it is interesting that the activity of the reused catalyst can basically maintain invariable in the temperature of 250–300 °C. In addition, the reused $CoFe_2O_4$/graphene-$_N$ do not significantly decrease the conversion of NO_x in the range of temperature from 300 °C to 400 °C.

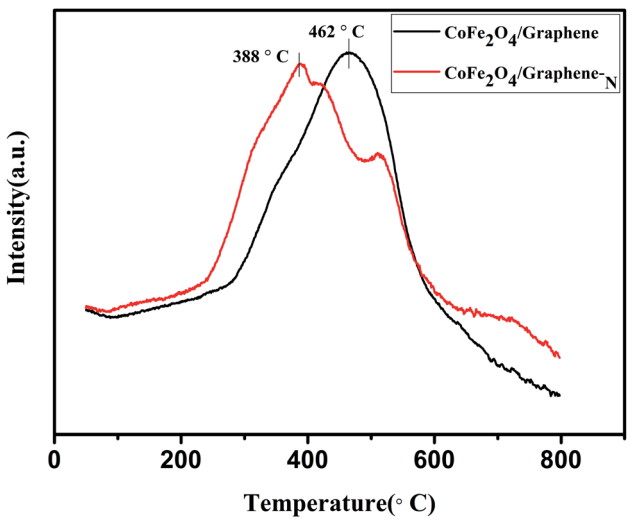

Fig. 7 H_2-TPR diagram of $CoFe_2O_4$/graphene and $CoFe_2O_4$/graphene-$_N$.

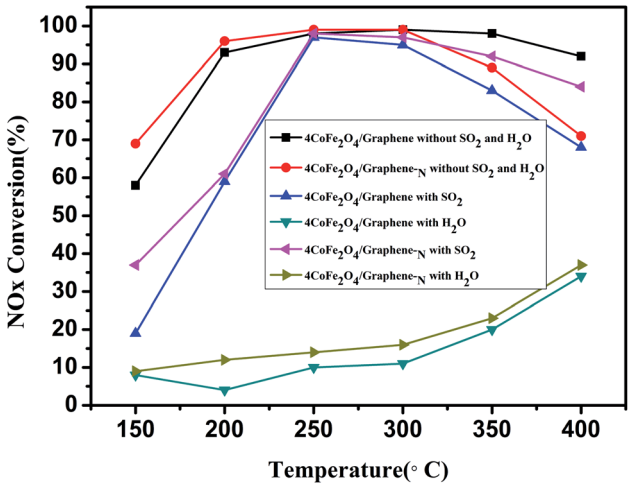

Fig. 8 The effect of SO_2 and H_2O on NO_x conversion over $CoFe_2O_4$/graphene and $CoFe_2O_4$/graphene-$_N$. Reaction conditions: NH_3 (500 ppm), NO (500 ppm), O_2 5%, SO_2 (100 ppm), H_2O 3%, N_2 as balanced gas, total gas flow (100 ml min^{-1}).

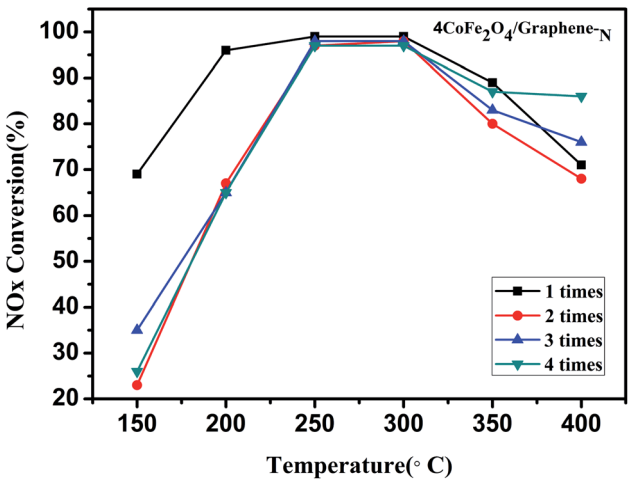

Fig. 9 Repeatability of $CoFe_2O_4$/graphene-$_N$ catalyst.

4. Conclusions

$CoFe_2O_4$/graphene catalysts and $CoFe_2O_4$/graphene-$_N$ catalysts were prepared. When the loading amount is 4%, the denitration activity of the catalysts is the best, and the conversion rate of NO_x reaches 99% at 250–300 °C. TEM showed that nitrogen doped made the distribution of the active components more uniform on the carrier. NH_3-TPD and H_2-TPR showed that nitrogen doped resulted in more acidic sites on the surface of the catalysts and improved the redox performance of the catalysts. $CoFe_2O_4$/graphene-$_N$ has better denitrification activity at low temperature than $CoFe_2O_4$/graphene, and the conversion rate of NO_x reaches more than 95% at 200–300 °C.

Conflicts of interest

There are no conflicts to declare.

Acknowledgements

This article was supported by National Natural Science Foundation of China (51708309), Heilongjiang Provincial Natural Science Foundation (QC2017065), The Fundamental Research Funds in Heilongjiang Provincial Universities (No. 135109103), Specialized Subject of Plant Food Processing Technology of Heilongjiang Education Department (YSTSXK201872), Qiqihar University Graduate Student Innovative Research Projects (YJSCX2018-032X).

References

1 K. W. Zha, S. X. Cai, H. Hu, H. R. Li, T. T. Yan, L. Y. Shi and D. S. Zhang, *J. Phys. Chem. C*, 2017, **121**, 25243–25254.
2 X. L. Li and Y. H. Li, *React. Kinet., Mech. Catal.*, 2014, **112**, 27–36.
3 H. Q. Wang, X. B. Chen, S. Gao, Z. B. Wu, Y. Liu and X. L. Weng, *Catal. Sci. Technol.*, 2013, **3**, 715–722.
4 X. Y. Shi, F. D. Liu, L. J. Xie, W. P. Shan and H. He, *Environ. Sci. Technol.*, 2013, **47**, 3293–3298.
5 J. Grzybek, B. Gil, W. J. Roth, M. Skoczek, A. Kowalczyk and L. Chmielarz, *Spectrochim. Acta, Part A*, 2018, **196**, 281–288.
6 C. Z. Shao, X. F. Liu, D. M. Meng, Q. Xu, Y. L. Guo, Y. Guo, W. C. Zhan, L. Wang and G. Z. Lu, *RSC Adv.*, 2016, **6**, 66169–66179.
7 C. A. Zhang, T. H. Chen, H. B. Liu, D. Chen, B. Xu and C. S. Qing, *Appl. Surf. Sci.*, 2018, **457**, 1116–1125.
8 W. L. Ma, H. Li, Q. Xu, Y. Zhang, W. Wang and J. D. Wang, *New J. Chem.*, 2018, **42**, 14757–14765.
9 J. M. Feng, X. H. Zhong, G. Z. Wang, L. Dong, X. F. Li and D. J. Li, *J. Mater. Sci.*, 2016, **52**, 3124–3132.
10 X. Y. Liu, Q. Li, J. N. Shu and H. Cui, *J. Mater. Chem. C*, 2017, **5**, 7612–7620.
11 N. Dong, F. Z. He, J. L. Xin, Q. Z. Wang, Z. Q. Lei and B. T. Su, *Mater. Res. Bull.*, 2016, **80**, 186–190.
12 M. Sundararajan, L. John Kennedy, P. Nithya and J. Judith Vijaya, *J. Phys. Chem. Solids*, 2017, **108**, 61–75.
13 B. Y. Ren, W. Shen, L. Li, S. Z. Wu and W. Wang, *Appl. Surf. Sci.*, 2018, **447**, 711–723.
14 P. A. Vinosha, B. Xavier, S. Krishnan and S. J. Das, *J. Nanosci. Nanotechnol.*, 2018, **18**, 5354–5366.
15 Q. A. Zhao, H. B. Zhao, L. Yan, M. X. Bi, Y. W. Li, Y. Q. Zhou, Z. J. Song and T. S. Jiang, *J. Nanosci. Nanotechnol.*, 2017, **17**, 3951–3958.
16 S. H. Wu, H. J. He, X. Li, C. P. Yang, G. M. Zeng, B. Wu, S. Y. He, L. Lu, *et al.*, *Chem. Eng. J.*, 2018, **341**, 126–136.
17 Y. J. Yao, Z. H. Yang, D. W. Zhang, W. C. Peng, H. Q. Sun and S. B. Wang, *Ind. Eng. Chem. Res.*, 2012, **51**, 6044–6051.
18 W. Y. Bian, Z. R. Yang, P. Strasser and R. Z. Yang, *J. Power Sources*, 2014, **250**, 196–203.
19 F. Yang, L. T. Jia, B. Hou, D. B. Li, J. G. Wang and Y. H. Sun, *J. Phys. Chem. C*, 2014, **118**, 268–277.
20 Y. B. Shao, T. Jing, J. Z. Tian and Y. J. Zheng, *RSC Adv.*, 2015, **5**, 103943–103955.
21 S. L. Ma, S. H. Zhan, Y. N. Jia and Q. X. Zhou, *ACS Appl. Mater. Interfaces*, 2015, **7**, 10576–10586.
22 Y. P. Dou, J. J. Peng, W. Li, M. Li, H. H. Liu and H. M. Zhang, *J. Nanopart. Res.*, 2015, **17**, 489.
23 C. R. Minitha and R. T. Rajendrakumar, *Adv. Mater. Res.*, 2013, **678**, 56–60.
24 P. Li, Z. F. Li, C. Geng, Y. Kang, C. Zhang and C. L. Yang, *Chin. J. Inorg. Chem.*, 2018, **34**, 2205–2210.
25 Y. Lin, S. H. Wu, X. Li, X. Wu, C. P. Yang, G. M. Zeng, Y. R. Peng, Q. Zhou and L. Lu, *Appl. Catal. B Environ.*, 2018, **227**, 557–570.
26 Y. Lin, S. H. Wu, C. P. Yang, M. Chen and X. Li, *Appl. Catal. B Environ.*, 2019, **245**, 71–86.
27 Q. Yuan, Z. Y. Zhang, N. S. Yu and B. Dong, *Catal. Commun.*, 2018, **108**, 23–26.
28 Q. J. Jin, Y. S. Shen, S. M. Zhu, X. H. Li and M. Hu, *Chin. J. Catal.*, 2016, **37**, 1521–1528.
29 W. Yan, Y. S. Shen, S. M. Zhu, Q. J. Jin, Y. L. Liu and X. H. Li, *Catal. Lett.*, 2016, **146**, 1221–1230.
30 S. L. Zhang, Q. Z. Jiao, J. Hu, J. J. Li, Y. Zhao, H. S. Li and Q. Wu, *J. Alloys Compd.*, 2015, **630**, 195–201.
31 L. X. Zheng, L. T. Guan, G. Yang, S. M. Chen and H. J. Zheng, *RSC Adv.*, 2018, **8**, 8607–8614.
32 F. Nie, J. J. Shi, W. C Du, W. S. Ning, Z. Y. Hou and F. S. Xiao, *J. Mater. Chem. A*, 2013, **1**, 9037–9045.
33 H. Xia, D. D. Zhu, Y. S. Fu and X. Wang, *Electrochim. Acta*, 2012, **83**, 166–174.
34 M. Zhang, X. Yang, X. F. Kan, X. Wang, L. Ma and M. Q. Jia, *Electrochim. Acta*, 2013, **112**, 727–734.
35 S. H. Li, H. Miao, Q. Xu, Y. J. Xue, S. S. Sun, Q. Wang and Z. P. Liu, *RSC Adv.*, 2016, **6**, 99179–99183.
36 E. J. Biddinger, D. von Deak and U. S. Ozkan, *Top. Catal.*, 2009, **52**, 1566–1574.
37 Y. Jiang, Z. M. Xing, X. C. Wang, S. B. Huang, Q. Y. Liu and J. S. Yang, *J. Ind. Eng. Chem.*, 2015, **29**, 43–47.
38 Z. M. Liu, S. X. Zhang, J. H. Li and L. L. Ma, *Appl. Catal. B Environ.*, 2014, **144**, 90–95.
39 H. F. Li, G. Z. Lu, Q. G. Dai, Y. Q. Wang, Y. Guo and Y. L. Guo, *Appl. Catal. B Environ.*, 2011, **102**, 475–483.
40 R. B. Jin, Y. Liu, Z. B. Wu, H. Q. Wang and T. T. Gu, *Catal. Today*, 2010, **153**, 84–89.
41 C. C. Xu, W. Sun, L. M. Cao, T. T. Li, X. X. Cai and J. Yang, *Chem. Eng. J.*, 2017, **308**, 980–987.